SUPPORTING INFORMATION APPENDIX FOR

Prefrontal-hippocampal functional connectivity encodes recognition memory and is impaired in intellectual disability

Maria Alemany-González, Thomas Gener, Pau Nebot, Marta Vilademunt, Mara Dierssen and M. Victoria Puig

SUPPORTING FIGURES

Figure S1. Classification of neurons as pyramidal and non-pyramidal in euploid and Ts65Dn mice.

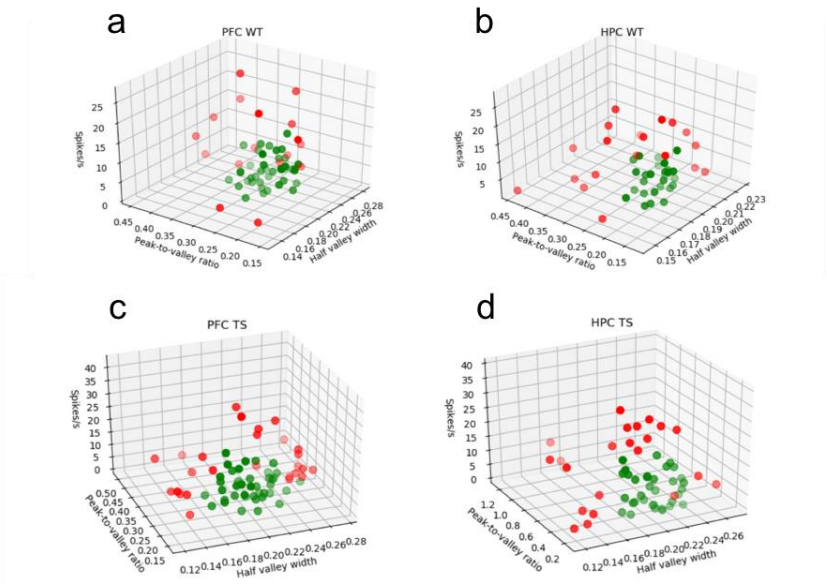

Figure S1. Neurons were classified based on three electrophysiological properties as in Kim *et al.* (Cell 2016): peak-to-valley ratio, half-valley width of action potentials and firing rate during resting states. Green dots denote putative pyramidal neurons (wide spiking) and red dots represent unclassified putative non-pyramidal neurons (narrow spiking). Shown are 3D plots of the three parameters in PFC **(a, c)** and HPC **(b, d)** of euploid and Ts65Dn mice.

Figure S2. Ts65Dn mice exhibit prefrontal-hippocampal hypersynchronization during quiet wakefulness in the open field.

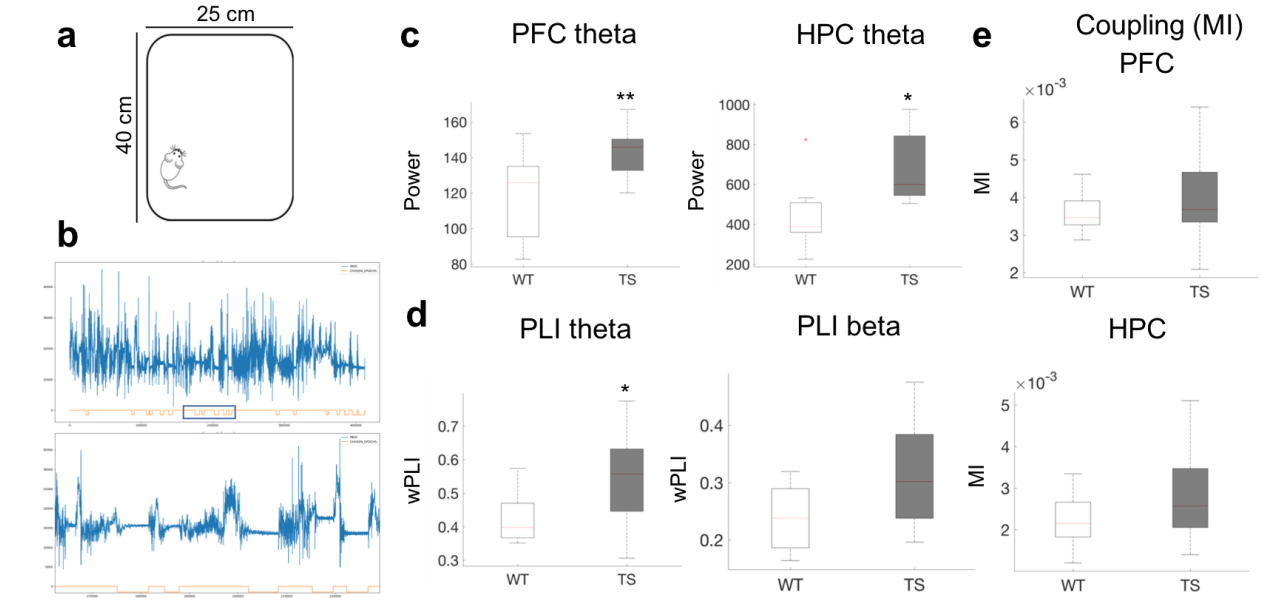

Figure S2. (a) Dimensions of the open field used. **(b)** Example of general activity (variance of the acceleration module, Acc) of a WT male mouse during an open field session. The orange line below represents the classification between resting and movement. We used resting epochs of minimum 3 consecutive seconds to investigate neural activity during quiet wakefulness. The rectangle epoch on the upper panel is expanded on the lower panel. **(c)** PFC and HPC theta power were increased in TS mice. **(d)** PFC-HPC theta and beta phase synchronization (wPLI) were increased in TS mice. **(e)** Cross-frequency coupling in the PFC (delta – high gamma) and HPC (theta – high frequency oscillations) was slightly stronger in TS mice. Data are represented as mean ± SEM (9 WT vs. 11 TS mice; unpaired T test, PFC theta: P = 0.01; HPC theta: P = 0.045; PLI theta: P = 0.049; PLI beta: P = 0.18; MI PFC: P = 0.54; MI HPC: P = 0.17).

Figure S3. Euploid and Ts65Dn mice exhibit similar cortical neuroinflammation due to craniotomies.

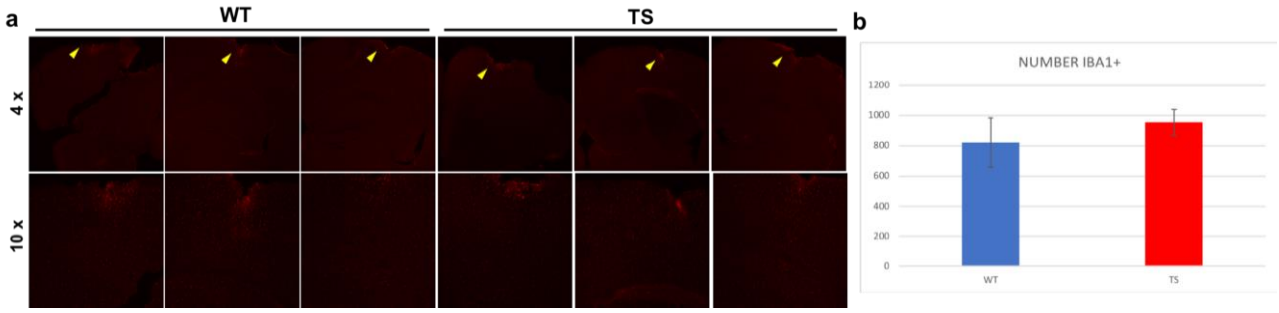

Figure S3. (a) We examined differential cortical neuroinflammation caused by craniotomies using immunostaining for Iba1 (Iba1 antibody from rabbit, donkey anti-rabbit secondary antibody; Wako) 10 days after electrode implantation in 3 WT and 3 TS male mice (shown is a representative immunostaining of each animal). **(b)** We quantified the number of Iba1+ cells with ImageJ in the cortical area below the craniotomy in regions of the same size in the 6 mice. The amount of Iba1+ cells was similar in the two genotypes (unpaired T test, P = 0.50).

Figure S4. Euploid and Ts65Dn mice exhibit similar myelination in the PFC, HPC and the anterior commissure (AC).

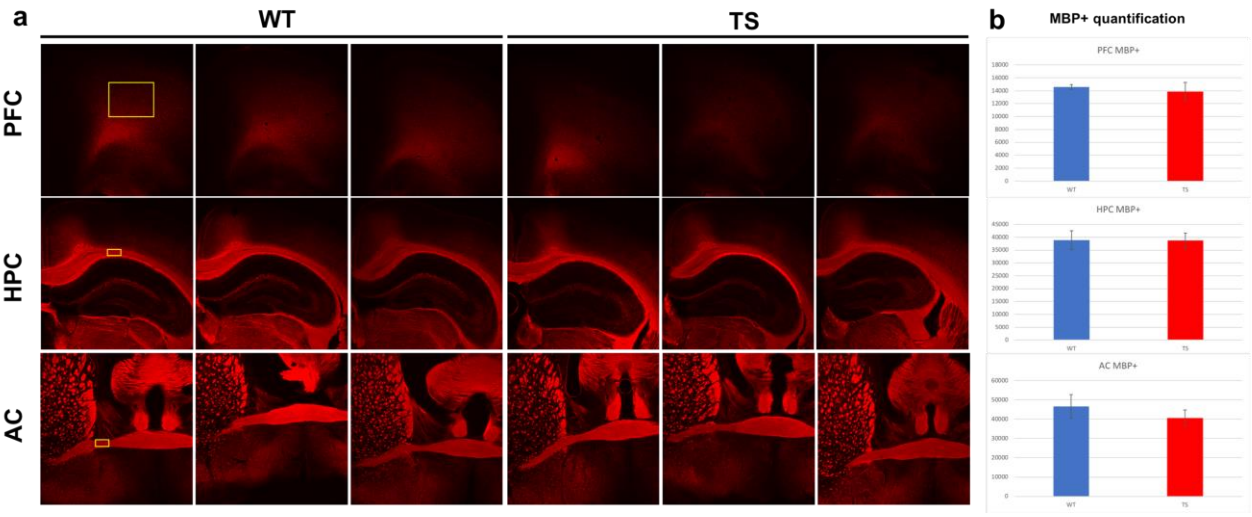

Figure S4. We examined differential myelination in the PFC, HPC and Anterior Commissure (AC) regions by immunostaining for MBP (myelin basic protein). We investigated the AC because is a key fiber tract that

reflects interhemispheric communication. We quantified MBP+ immunodensity by measuring the mean grey value in WT and TS mice. (**a)** Representative immunostaining of myelin using MBP (MBP antibody from rabbit, donkey anti-rabbit secondary antibody) in the PFC (upper), HPC (middle) and AC (lower) in 3 WT and 3 TS male mice (shown is a representative immunostaining of each animal). **(b)** Quantification of MBP+ immunodensity by measuring the mean grey value in the PFC, HPC and AC in WT and TS mice. The amount of myelination was comparable across genotypes (3 WT vs. 3 TS mice; unpaired T test, PFC: P = 0.64; HPC: P = 0.99; AC: P = 0.4).

Figure S5. Euploid and Ts65Dn mice exhibit similar body temperature regulation before, during and after 10 days of oral treatment with EGCG.

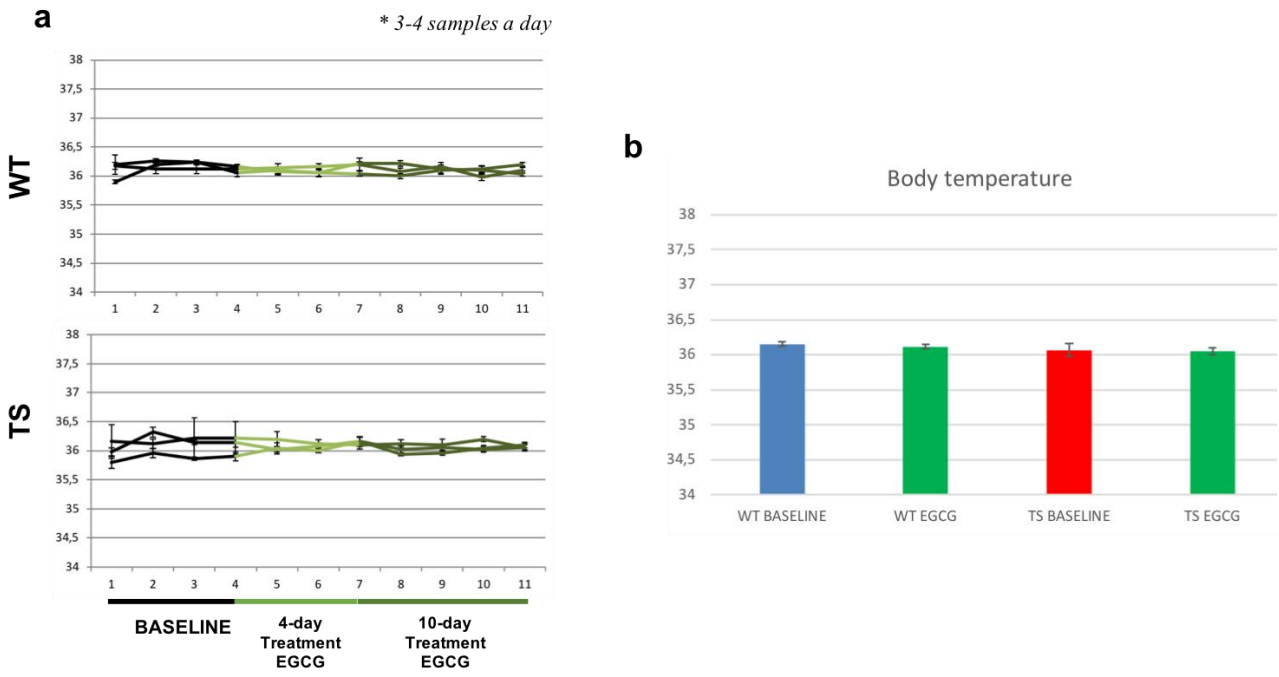

Figure S5. We measured body temperature (3-4 samples a day) in 3 WT and 3 TS male mice with a digital thermometer (via light illumination on skin around the rectum) with the minimal handling possible to avoid influence of animals' stress on the readings. We collected 3-4 samples a day (1.5 hours apart) before and after 4- and 10-day treatment with EGCG in the drinking water. **(a)** Body temperature of each mouse and timestamp at baseline conditions and after 4 and 10 days of treatment with oral EGCG in 3 WT (upper panel) and 3 TS mice (lower panel). The body temperature was very consistent over time and was not affected by EGCG. **(b)** Quantification of body temperature in WT and TS mice at baseline conditions and after 10 days of treatment

with EGCG. We conclude from our observations that body temperature of our colony under our experimental setting was similar over different days and across genotypes (WT = 36.15; TS = 36.06; unpaired T test, P = 0.46) and that EGCG did not induce changes in body temperature on either group (paired T test, WT: P = 0.44; TS: P = 0.87).

Figure S6. The beneficial effects of EGCG in Ts65Dn mice are transient.

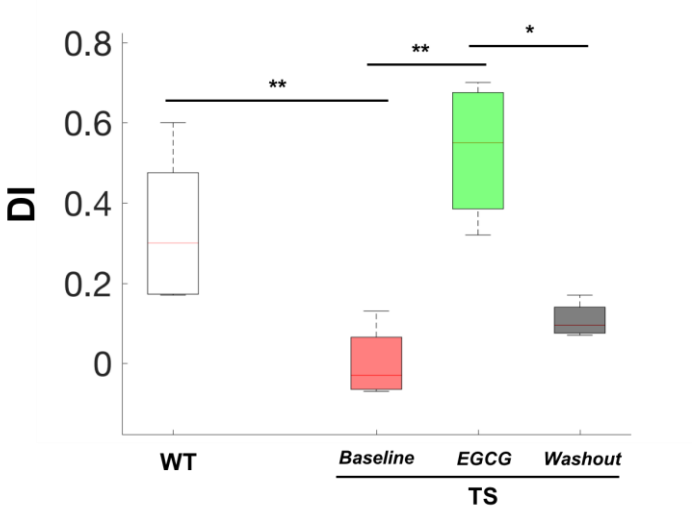

Figure S6. We assessed memory abilities in the five responder TS mice one month after the treatment had subsided to investigate the temporal effects of EGCG. During baseline, discrimination indexes of TS mice were lower than those of WT mice (WT n = 10 vs. TS n = 11 mice; unpaired T test, P = < 0.00005). One month of oral treatment with EGCG markedly ameliorated memory abilities of TS mice (TS n = 8 mice; paired T test, P = 0.02). However, responder mice performed worse after EGCG had washed out (DIs 5 TS mice baseline, EGCG and washout; ANOVA $F_{2,6}$ = 16.21, P = 0.004 with Bonferroni correction for multiple comparisons) pointing to transient effects of EGCG.

SUPPORTING TABLES

Table S1. Classification of neurons as pyramidal and non-pyramidal in euploid and Ts65Dn mice. Quantification of neurons shown in Supporting Figure 1. N denotes the number of individual neurons included in the analysis per brain area and genotype.

Genotype	Area	N pyr	N non pyr	% Pyr
WT	PFC	41	17	70,69
WT	HPC	28	20	58,33
TS	PFC	40	26	60,61
TS	HPC	34	22	60,71

This study generated a large dataset that has been summarized in three Supporting Tables. Figures in the main text show only the neurophysiological parameters that were different between wild-type and Ts65Dn mice in each brain state (quiet wakefulness, NREM and REM sleep, memory performance) before and after EGCG (Ts65Dn mice only).

Table S2. Distinct neural activities in prefrontal-hippocampal circuits of WT and Ts65Dn mice during quiet wakefulness and sleep, and effects of chronic EGCG

Shown are neural activities quantified during quiet wakefulness, NREM and REM sleep in WT and TS mice. Red and blue denote differences between genotypes (red: increased in TS mice vs. WT mice; blue: decreased in TS mice vs. WT mice; unpaired T tests). Green represents normalization by EGCG in the 6 responder TS mice (paired T tests). Results are represented by mean and SEM.

		QUIET WAKE								NREM SLEEP								REM SLEEP							
	BAND	WT (n=10)		TS (n=12)		P WT vs. TS	TS EGCG (n=6)		P EGCG effect	WT (n=10)		TS (n=12)		P WT vs. TS	TS EGCG (n=5)		P EGCG effect	WT (n=8)		TS (n=11)		P WT vs. TS	TS EGCG (n=3)		P EGCG effect
		Mean	SEM	Mean	SEM		Mean	SEM		Mean	SEM	Mean	SEM		Mean	SEM		Mean	SEM	Mean	SEM		Mean	SEM	
Power PFC	Delta	649.54	111.52	659.36	85.50	0.94	635.70	135.24	0.53	**2562.01**	**392.10**	**1556.47**	**251.62**	**0.03**	2446.98	1142.89	0.73	235.21	37.21	180.99	25.19	0.23	318.03	126.17	0.40
	Theta	**164.08**	**10.08**	**196.91**	**10.71**	**0.04**	**161.73**	**14.05**	**0.03**	312.67	23.75	303.59	26.66	0.80	278.91	35.25	0.95	**108.51**	**9.38**	**223.31**	**33.21**	**0.006**	159.82	52.20	0.84
	Beta	27.71	1.30	29.02	1.41	0.51	31.38	2.99	0.47	35.70	1.36	39.79	3.38	0.35	35.63	3.80	0.80	**27.31**	**2.73**	**41.26**	**4.02**	**0.01**	28.76	4.68	0.29
	Low Gamma	12.54	0.88	12.02	0.77	0.65	12.56	2.50	0.55	**7.48**	**0.24**	**9.39**	**0.66**	**0.01**	7.59	0.60	0.40	10.88	0.70	13.48	1.18	0.12	12.83	3.42	0.82
	High Gamma	6.87	0.41	6.99	0.49	0.84	6.91	1.14	0.70	3.39	0.24	4.04	0.33	0.13	3.46	0.29	0.51	5.97	0.59	5.24	0.33	0.28	6.46	1.72	0.87
MI PFC	Delta-High Gamma	**1.43E-04**	**0.00003**	**8.53E-04**	**0.0003**	**0.04**	8.57E-04	0.0008	0.35	6.55E-04	0.00004	4.28E-04	0.00003	0.10	9.33E-02	0.04	0.11	7.41E-04	0.00003	7.50E-04	0.00002	0.92	0.34	0.19	0.03
Power HPC	Delta	720.46	64.12	1117.67	200.44	0.08	1469.11	276.57	0.54	2464.37	287.59	2217.99	533.34	0.68	4380.35	978.48	0.29	526.30	102.43	336.26	59.92	0.11	703.80	119.85	0.97
	Theta	**714.64**	**101.28**	**1197.99**	**195.97**	**0.04**	1239.59	347.67	0.99	832.49	90.48	1111.76	192.77	0.20	1761.22	332.14	0.13	790.68	131.72	664.86	102.43	0.45	727.36	111.14	0.96
	Beta	125.24	19.02	147.99	18.74	0.40	172.12	31.04	0.99	186.01	26.01	186.73	26.77	0.98	296.26	64.02	0.14	137.58	29.17	133.51	19.87	0.90	175.72	12.41	0.15
	Low Gamma	53.25	6.16	69.85	9.87	0.17	71.41	11.43	0.20	47.72	6.55	58.19	9.50	0.39	71.89	12.96	0.93	44.81	7.47	52.44	9.45	0.55	79.44	10.62	0.32
	High Gamma	21.28	2.12	28.79	5.39	0.21	28.98	4.73	0.18	14.82	2.00	18.44	3.22	0.36	25.80	4.77	0.58	20.61	2.87	24.68	5.05	0.49	32.68	4.10	0.05
MI HPC	Theta-HFO	**2.27E-04**	**0.00005**	**4.90E-04**	**0.00008**	**0.03**	1.45E-04	0.00009	0.19	2.38E-03	0.0002	2.69E-03	0.0002	0.68	2.54E-03	0.0003	0.71	2.35E-03	0.04	3.54E-03	0.03	0.13	3.16e-05	0.00005	0.13
Ripples HPC	Power									**0.13**	**0.04**	**0.17**	**0.05**	**0.04**	**0.15**	**0.02**	**0.04**								
	Frequency									**104.84**	**33.15**	**100.00**	**31.62**	**0.03**	116.88	8.53	0.16								
wPLI PFC-HPC	Delta	**0.36**	**0.01**	**0.43**	**0.03**	**0.03**	0.46	0.05	0.22	0.50	0.02	0.53	0.01	0.24	0.53	0.01	0.66	0.55	0.04	0.60	0.04	0.41	0.52	0.08	0.001
	Theta	**0.22**	**0.003**	**0.31**	**0.03**	**0.01**	0.29	0.03	0.23	**0.46**	**0.02**	**0.51**	**0.01**	**0.03**	0.52	0.03	0.19	0.33	0.03	0.36	0.03	0.51	0.34	0.08	0.97
	Beta	**0.22**	**0.003**	**0.25**	**0.01**	**0.03**	0.26	0.02	0.16	0.38	0.02	0.41	0.01	0.17	0.40	0.01	0.61	0.21	0.02	0.22	0.01	0.69	0.24	0.03	0.57
	Low Gamma	0.23	0.003	0.23	0.004	0.62	0.25	0.01	0.18	0.30	0.02	0.34	0.01	0.14	0.33	0.02	0.85	**0.19**	**0.02**	**0.26**	**0.01**	**0.009**	0.27	0.03	0.70
	High Gamma	0.18	0.004	0.19	0.008	0.60	0.20	0.01	0.54	0.26	0.02	0.29	0.01	0.28	0.29	0.03	0.90	0.19	0.02	0.21	0.01	0.45	0.23	0.03	0.92

Table S3. Neural activities of prefrontal-hippocampal circuits associated with object memory acquisition/novelty, familiarization and retrieval in WT mice.

Shown are neural activities quantified during early and late explorations in the familiarization phase and during familiar and novel explorations in the 24-hour memory test in WT mice. Orange denotes significant differences between early and late explorations and between novel and familiar explorations of objects (paired T tests).

WT		FAMILIARIZATION (n=10)					24-HOUR MEMORY TEST (n=10)				
	BAND	EARLY		LATE		P	NOVEL		FAMILIAR		P
		Mean	SEM	Mean	SEM		Mean	SEM	Mean	SEM	
Power PFC	Theta	**761.97**	**167.57**	**325.77**	**35.06**	**0.02**	267.41	32.16	346.50	65.89	0.30
	Beta	43.14	5.38	37.66	3.73	0.22	41.01	5.23	40.43	4.14	0.89
	Low Gamma	17.02	1.55	15.13	0.71	0.18	15.82	0.82	15.46	0.95	0.74
	High Gamma	**8.65**	**0.68**	**7.90**	**0.54**	**0.04**	8.19	0.36	7.94	0.46	0.43
Power HPC	Theta	**1390.72**	**219.99**	**1089.00**	**184.95**	**0.02**	995.25	139.96	1274.67	242.63	0.05
	Beta	155.41	25.32	173.27	32.79	0.23	158.61	25.28	179.37	30.22	0.07
	Low Gamma	57.42	7.04	61.40	8.53	0.18	**61.74**	**28.58**	**56.62**	**23.47**	**0.005**
	High Gamma	34.55	3.79	34.27	4.42	0.89	32.74	4.08	29.39	4.64	0.25
wPLI PFC-HPC	Theta	0.67	0.06	0.68	0.04	0.93	0.68	0.05	0.68	0.05	0.92
	Beta	0.35	0.04	0.42	0.05	0.22	0.37	0.02	0.35	0.03	0.39
	Low Gamma	**0.23**	**0.02**	**0.31**	**0.02**	**0.003**	0.22	0.03	0.22	0.02	0.98
	High Gamma	0.20	0.01	0.17	0.01	0.13	**0.20**	**0.02**	**0.12**	**0.03**	**0.01**
PSI PFC-HPC	Theta	**0.67**	**0.27**	**-0.83**	**0.24**	**0.002**	-0.56	0.75	-0.34	0.77	0.82
	Beta	-0.22	0.50	0.40	0.70	0.44	-0.16	0.53	0.93	0.32	0.14
	Low Gamma	-1.13	1.27	-0.31	1.00	0.58	**-1.20**	**0.62**	**4.86**	**1.91**	**0.01**
	High Gamma	0.19	1.55	-0.08	1.17	0.89	3.14	1.73	-2.57	3.07	0.23

Table S4. Neural activities of prefrontal-hippocampal circuits associated with memory acquisition /novelty, familiarization and retrieval in TS mice and effects of chronic EGCG.

Shown are neural activities quantified during early and late explorations in the familiarization phase and during familiar and novel explorations in the 24-hour memory test in TS mice. Highlighted cells denote significant differences with the WT mice ratios reported in Supporting Table 3. In green we hallmark those measures normalized in TS mice after EGCG. The two measures that reflect hypersynchronization during familiar object explorations in TS mice (fig. 3f of main text) are underlined: HPC low gamma power (familiar explorations in WT mice vs. TS mice; unpaired T test, P = 0.04) and PFC-HPC high gamma wPLI (P = 0.049).

TS		FAMILIARIZATION										24-HOUR MEMORY TEST									
		TS pre-EGCG (n=9)					TS post-EGCG (n=5)					TS pre-EGCG (n=9)					TS post-EGCG (n=5)				
	BAND	EARLY		LATE		P	EARLY		LATE		P	NOVEL		FAMILIAR		P	NOVEL		FAMILIAR		P
		Mean	SEM	Mean	SEM		Mean	SEM	Mean	SEM		Mean	SEM	Mean	SEM		Mean	SEM	Mean	SEM	
Power PFC	Theta	543.66	109.03	307.27	65.82	0.13	**807.35**	**141.20**	**307.14**	**74.85**	**0.03**	463.91	129.85	358.25	59.95	0.47	277.58	41.56	347.69	79.24	0.25
	Beta	42.24	4.11	36.03	3.76	0.24	77.26	13.49	35.57	3.21	0.03	51.18	9.32	56.94	18.78	0.79	36.24	5.09	46.09	11.03	0.25
	Low Gamma	18.07	2.34	15.13	1.98	0.03	21.54	2.51	16.59	2.19	0.21	19.03	2.42	19.98	2.63	0.69	16.08	2.59	17.86	2.44	0.22
	High Gamma	8.93	1.03	8.57	1.11	0.53	9.95	0.92	8.43	0.85	0.09	9.14	0.78	9.12	0.76	0.95	8.57	1.02	8.65	1.03	0.94
Power HPC	Theta	1478.48	305.98	1021.40	124.15	0.11	**2587.25**	**748.44**	**1690.95**	**594.63**	**0.03**	1309.30	341.90	1332.91	323.72	0.74	1657.26	501.81	1787.43	607.02	0.31
	Beta	171.55	35.59	156.51	20.73	0.53	241.55	51.75	197.52	39.24	0.14	183.92	39.68	212.84	44.76	0.32	193.95	50.10	207.41	46.87	0.27
	Low Gamma	91.74	19.62	100.77	20.06	0.33	79.88	18.03	88.61	16.81	0.16	**93.86**	**17.49**	**88.66**	**14.61**	**0.34**	**80.28**	**18.66**	**70.36**	**15.11**	**0.15**
	High Gamma	45.35	11.27	45.74	11.56	0.95	47.87	11.11	45.27	9.41	0.62	41.90	10.10	45.01	10.61	0.29	38.46	9.40	40.07	9.58	0.18
wPLI PFC-HPC	Theta	0.58	0.06	0.68	0.07	0.25	0.62	0.08	0.73	0.11	0.21	0.74	0.05	0.77	0.04	0.57	0.72	0.06	0.62	0.09	0.12
	Beta	0.36	0.03	0.28	0.04	0.01	0.32	0.05	0.43	0.06	0.23	**0.42**	**0.03**	**0.30**	**0.04**	**0.02**	0.36	0.04	0.43	0.06	0.32
	Low Gamma	**0.23**	**0.02**	**0.25**	**0.01**	**0.4**	**0.25**	**0.02**	**0.25**	**0.04**	**0.99**	0.24	0.03	0.20	0.04	0.25	0.25	0.02	0.24	0.04	0.89
	High Gamma	0.24	0.03	0.17	0.02	0.08	0.17	0.03	0.19	0.02	0.60	**0.19**	**0.02**	**0.21**	**0.03**	**0.48**	**0.23**	**0.01**	**0.15**	**0.01**	**0.02**
PSI PFC-HPC	Theta	**-0.16**	**0.48**	**-0.10**	**0.37**	**0.92**	**0.62**	**0.86**	**-1.43**	**0.44**	**0.02**	-0.16	0.31	-0.41	0.55	0.63	-1.03	0.34	-1.76	0.94	0.32
	Beta	1.39	0.69	-1.23	0.69	0.04	-0.61	0.81	0.96	0.70	0.16	0.81	0.60	-1.05	1.09	0.15	0.98	0.31	-0.73	0.54	0.06
	Low Gamma	-1.48	0.95	0.83	1.30	0.22	0.20	1.67	-1.42	1.67	0.64	**-1.35**	**1.66**	**-0.75**	**0.90**	**0.67**	**-0.72**	**0.60**	**2.88**	**0.89**	**0.02**
	High Gamma	1.07	1.24	1.14	1.34	0.97	-2.15	1.90	1.70	2.39	0.34	1.79	1.93	4.20	2.13	0.42	0.35	1.23	1.98	1.79	0.37

Table S5. Multiple regression modeling

Multiple regression models aimed to estimate the relative contribution of PFC theta power during rest, PFC-HPC theta PSI during object familiarization and PFC-HPC low gamma PSI during memory retrieval to memory performance (DIs) in WT, TS mice and TS mice treated with EGCG. Multiple regression models predicted DIs with high accuracy when combining the three parameters in WT mice ($F_{3,4}$ = 27.44, P = 0.004, R2 = 0.95). By contrast, they were not able to predict memory performance in TS mice ($F_{3,4}$ = 0.082, P = 0.96, R2 = 0.052), with marginal contribution of the three variables. In the 5 responder TS mice multiple regression models predicted DIs with high accuracy ($F_{3,4}$ = 1809, P = 0.01, R2 = 1).

Dependent Variable	Independent Variables	Model R^2	Model Adj. R^2	Model p- value	Beta Coefficient (stded)	Beta p-value
Discrimination Index	Full model	0.95	0.91	0.004	-	-
WT	PFC theta	-	-	-	-0.52	0.009
	PFC- HPC PSI theta	-	-	-	-0.58	0.01
	PFC- HPC PSI low gamma	-	-	-	0.47	0.02
Discrimination Index	Full model	0.05	-0.64	0.96	-	-
TS	PFC theta	-	-	-	0.08	0.89
	PFC-HPC PSI theta	-	-	-	0.24	0.70
	PFC-HPC PSI low gamma	-	-	-	0.003	0.99
Discrimination Index	Full model	1.00	0.99	0.01	-	-
TS post-EGCG	PFC theta	-	-	-	-0.96	0.02
	PFC-HPC PSI theta	-	-	-	-0.15	0.12
	PFC-HPC PSI low gamma	-	-	-	0.85	0.01

SUPPORTING METHODS

FULL METHODS

Animals

Ts65Dn male mice (TS, n = 12) and their wild-type littermates (WT, n = 10) were obtained by breeding B6EiC4Sn.BLiA-Ts(1716)65Dn/DnJ females with C57BL/6 × 6JOlaHsd (B6C3F1/OlaHsd) hybrid males. The parental generation was obtained from the Jackson Laboratory (Bar Harbor, ME) and a colony was generated and maintained at the Barcelona Biomedical Research Park (PRBB) Animal Facility. Female Ts65Dn mice used to create the parental generation were first generation of a Jax colony with stock number 001924. Mice were genotyped and ~25% of the offspring presented trisomy. Aged-matched euploid littermates served as controls. Animals were 2 to 3 months old at the start of all experiments and weighed between 20 to 30 g. Mice were housed on a conventional 12:12 light cycle, with lights on at 8 AM. Behavioral testing and recordings were conducted during the light phase of the circadian cycle, between 8 AM and 8 PM. All experiments were carried out at room temperature that was continuously monitored and maintained between 18-22 ºC. All procedures had authorization from the Barcelona Biomedical Research Park Animal Research Ethics Committee (PRBB-CEEA) and the local government (Generalitat de Catalunya) and were conducted according to the European Directive 2010/63/EU and Spanish regulations RD 53/2013.

Experimental Design

Mice were implanted with microelectrodes at 2-3 months of age. After a post-surgical recovery period, neural activity was recorded during several brain states (quiet wakefulness, REM and non REM sleep). Later, object recognition memory and its neurophysiological correlates were assessed. Then, epigallocatechin-3-gallate (EGCG) was administered for one month in the drinking water. Afterwards, a behavioral and neurophysiological characterization was performed as in pre-EGCG epochs. Finally, mice were euthanized and electrode placements were confirmed histologically (Fig. 1a of main text).

Surgery

Mice were anesthetized with a mixture of ketamine/xylazine (ketamine: Imalgene 1000, Distrivet SA; xylazine: X1251-1G, Sigma-Aldrich) and placed in a stereotaxic apparatus. Anesthesia was maintained with continuous 0.5-4% isoflurane (Zoetis Spain, S.L). Small craniotomies were drilled above the medial PFC and the HPC. Five micro-screws were screwed into the skull to stabilize the implant, and the one on top of the cerebellum was used as a general ground. Three tungsten electrodes, one stereotrode and one single electrode, were implanted in the PFC and three more were implanted in the HPC. The electrodes were positioned stereotaxically in the prelimbic PFC (AP: 1.5, 2.1 mm; ML: ± 0.6, 0.25 mm; DV: -1.7 mm from bregma) and in the CA1 area of the HPC (AP: -1.8, -2.5 mm; ML: -1.3, -2.3 mm; DV: -1.15, -1.25 mm). In addition, three reference electrodes were implanted in corpus callosum and lateral ventricles (AP: 1, 0.2, -1; ML: 1, 0.8, 1.7; DV: -1.25, -1.4, -1.5, respectively). The electrodes were made by twisting a strand of tungsten wire 25 μm wide (Advent, UK), had impedances that ranged from 100 to 400 kOhm at the time of implantation and were implanted unilaterally with dental cement. Electrode wires were pinned to an adaptor to facilitate their connection to the recording system. After surgery animals were allowed to recover during at least one week. Animals were housed individually in cages with high lids after the surgery and throughout the experiment to avoid damage to their implants. After the experiments ended, a mild electrical current (100 Hz, 0.1 mA, 2 s) was applied to the electrodes to mark the placement of electrode tips, which were later confirmed histologically by staining the brain slices with Cresyl violet (Sigma-Aldrich) (Fig. 1a of main text). Electrodes with tips outside the targeted areas were discarded from data analyses.

Behavioral and Neurophysiological Characterization

We recorded single-unit activity (SUA) and local field potentials (LFPs) in freely-moving mice with the multi-channel Open Ephys system at a sampling rate of 30 kHz with Intan RHD2132 amplifiers equipped with an accelerometer. We assessed general mobility of mice as in Gener et al., 2019. We quantified the instantaneous module of the data recorded by the accelerometer in the x, y and z axis downsampled from 30 kHz to 1 kHz. We then calculated the variance of the module over one-minute bins to obtain a useful measure that keeps track of the general mobility of mice during the experiments. The Acc is sensitive enough to reflect differences in mobility between sleep states and sedation (Gener et al., 2019). In addition, recorded signals from each

electrode were filtered offline to extract SUA and LFPs. SUA was estimated by first subtracting the raw signal from each electrode with the signal from a nearby referencing electrode to remove artifacts related to animal´s movement. Next, referenced signals were filtered between 450-6000 Hz and the spikes from individual neurons were sorted using principal component analysis with Offline Sorter v4 (Plexon Inc.). To obtain LFPs, signals were downsampled to 1 kHz, detrended and notch-filtered to remove noise line artifacts (50 and 100 Hz) with custom-written scripts in Python. Signals were then imported into MATLAB (MathWorks, Natick, MA). The frequency bands considered for the band-specific analyses included delta (1-4 Hz), theta (8-12 Hz), beta (18-25 Hz), low gamma (30-50 Hz), and high gamma (50-80 Hz).

Quiet Wakefulness, NREM and REM Sleep

Recordings during quiet wakefulness were performed while the animals were constrained to a small box (12 cm * 8 cm) that allowed them to move but not to walk. Muscle tone and motor activity were thus present but active exploration (locomotion) was prevented. Recordings during the open field were performed in a 40 x 25 cm box where the animals could move freely. More natural (i.e., less stressful) resting episodes of 3 consecutive seconds or more were identified by setting a threshold to the Acc to detect epochs of low mobility (Fig. S2b). More specifically, quiet epochs were detected using a custom-made script in Python. The algorithm computed the absolute difference between each pair of consecutive accelerometer module points. Then, a Savitzky–Golay filter (order = 0, window = 100 ms) was applied to extract the trend aside from minor variations, followed by the application of a threshold and later grouping of time points detected as low mobility. The selected threshold and posterior joining distance were chosen by observation of quiet epochs on video recordings and their respective accelerometers (considered quiet if the module difference was less than 60 and joining epochs separated less than 500 ms). Recordings during natural sleep were implemented following the familiarization phase of the NOR task to better capture neural signals related to memory consolidation. Accelerometer measures and LFP signals from the PFC and the HPC were used to classify epochs of REM and NREM sleep. NREM sleep was defined as animal immobility (low variations of the accelerometer) and large amplitude slow oscillations (1-4 Hz) in the PFC and HPC. Only periods of NREM sleep prior to REM episodes were considered for analysis. REM sleep epochs were defined as animal immobility and prominent hippocampal theta rhythms (Fig. 2a of main text). Analyses of LFPs signals during quiet wakefulness and

natural sleep were performed averaging neural signals over discrete epochs of different duration (one continuous epoch per experiment; quiet wakefulness: 3 min; NREM sleep: 1 min; REM sleep: 10 s) that were chosen based on the stability of the brain state (McShane et al., 2012).

The Novel Object Recognition Task

We tested recognition memory using a well-established task that relies on mice innate instinct to explore novel objects in the environment (McShane et al., 2012). We used a custom-designed T-maze made of aluminum with wider and higher arms than the standard mazes (8 cm wide x 30 cm long x 20 cm high). The maze was shielded and grounded for electrophysiological recordings and was placed on an aluminum platform. The novel-familiar object pairs were previously validated as in (Gulinello et al., 2018). The arm of the maze where the novel object was placed was randomly chosen across experiments. The test was implemented in three phases of 10 minutes each: habituation and familiarization during the first day and long-term memory test 24 hours after familiarization. Mice were first habituated to an empty maze. Five minutes later, mice were placed again in the maze where they could explore two identical objects located at the end of the two lateral arms. Twenty-four hours later, in the test phase, mice were presented with one familiar and one novel object (Fig. 3a of main text). Each session was videotaped via a video camera located on top of the maze. We recorded electrophysiological activity continuously during the full ten minutes of familiarization and memory tests of the NOR task. Any investigative behavior of objects, including head orientation towards the objects or sniffing at a distance below or equal to 2 cm or when the mice touched the objects with the nose, was considered object exploration. Exploratory events were identified online by looking at the video using a custom-designed joystick with a right and left button that were pressed continuously during the time of explorations. Button presses were automatically aligned to the electrophysiological file by sending TTL pulses to the acquisition system so that two more event channels were added to the recording files (Fig. 3d of main text). Object recognition memory was defined by the discrimination index (DI) for the novel object using the difference in exploration time for the familiar object divided by the total amount of exploration of both objects (DI = [Novel Object Exploration Time-Familiar Object Exploration Time]/Total Exploration Time). DIs vary between +1 and -1, where a positive score indicates more time spent with the novel object, a negative score indicates more time spent with the familiar object, and a zero score indicates a null preference (Leger et al., 2013).

LFP measures associated with memory acquisition and retrieval were obtained by averaging one-second non-overlapping windows triggered by the button presses on the joystick. Each one-second window was only considered if the mouse explored the object over 600 ms. This allowed us to include many interactions from TS mice that were particularly short (Fig. 3c of main text) while also granting a good estimation of power at low frequencies. Memory acquisition was investigated during the familiarization phase when the two objects were identical. We ordered the explorations of the two objects in time and compared neural activity during the first 5 vs. the last 5 seconds of exploration (i.e., 5 early vs. 5 late one-second windows). Memory retrieval was investigated during the 24-hour memory test by comparing neural signals during explorations of familiar versus novel objects (Fig. 3b of main text). This implied that more one-second windows could be included for WT than for TS mice, as TS mice typically explored novel and familiar objects for short periods of time, despite the total number of explorations was similar (Fig. 3c of main text). We found that these criteria provided the most robust results.

EGCG Treatment

Mice were administered EGCG in drinking water for one month. EGCG solution was prepared freshly from a green tea leaf extract [Mega Green Tea Extract, Decaffeinated, Life Extension®, USA; 45% extract with an EGCG content of 326.25 mg per capsule] every 3 days (EGCG concentration: 90 mg/mL for a dose of 2–3 mg per day). EGCG was administered 2-3 weeks after surgery following an initial behavioral and electrophysiological characterization of mice (Fig. 1a of main text).

Data Analyses

All analyses were carried out with custom scripts programmed in Python (data pre-processing, Acc) and MATLAB (power, cross-frequency modulation index, ripples, wPLI, PSI), except spike sorting that was performed with Offline Sorter version 4. Except Acc (general activity of mice) (Gener et al., 2019), all the functions used in our analyses have been developed and validated by other laboratories.

Power Spectral Analyses. We used the multitaper fast Fourier transform method (time frequency bandwidth; TW = 5 and K = 9 tapers; 1-100 Hz range; non-overlapping sliding window of 5 seconds for power spectra, 2

seconds for spectrograms, 1 second for object explorations) with the Chronux toolbox (Bokil et al., 2010) in MATLAB version 2.12 that is available at http://chronux.org. Power spectra were estimated with the Chronux function *mtspectrumc*.

Phase-Amplitude Modulation index. To quantify the intensity of phase-amplitude coupling we used the modulation index (MI) as described in Tort et al. 2010. First, low frequency (delta and theta) phases were divided into 18º bins and gamma (low, high gamma and high frequency oscillations-HFO) amplitude was calculated for each phase bin. MI measures the divergence of the phase-amplitude distribution and is higher as further away is from the uniform distribution. In order to choose specific frequency bands pairs for the MI quantification we represented overall MI in a two-dimensional pseudocolor comodulation map. A warmer color indicates coupling between the phase of the low frequency band (x axis) and the amplitude of the high frequency band (y axis) while blue depicts absence of coupling. We used the modulation index function from Tort et al. 2010 that is available at:
https://github.com/cineguerrilha/Neurodynamics/blob/master/16ch/Comodulation/ModIndex_v1.m

Weighted Phase Lag Index (wPLI). To assess functional connectivity between LFPs in the PFC and HPC we used the wPLI as in Vinck et al., 2011 and Hardmeier et al., 2014. First, instantaneous phases from LFP signals recorded simultaneously in both areas were determined by Hilbert transformation. wPLI measures the asymmetry in the distribution of phase differences for each frequency band between the two time-series resulting in values ranging between 0 and 1, being a higher value a high asymmetric distribution as a consequence of a consistent phase-lag between signals in the two areas. wPLI reduces the probability of detecting false positive connectivity in the case of volume conducted noise sources with near zero phase lag and shows higher sensitivity in detecting real phase synchronization. It was estimated with a Butterworth filter of order 3 with a script provided by A. Tauste as in Gener et al. 2019.

Phase Slope Index (PSI). To estimate the flow of information between neural signals of the PFC and HPC, we used the Phase Slope Index as in Nolte et al., 2008. PSI is a robust measure based on the conceptual temporal argument supporting that the driver is earlier than the recipient and contains information about the

future of the recipient. It quantifies the consistency of the direction of the change in the phase difference across frequencies. Positive slope reflects an HPC-to-PFC flow of information in a specific frequency range while a negative slope reflects the opposite. We used the function from Nolte et al. 2008 that is available here: http://doc.ml.tu-berlin.de/causality/

***Analyses of ripples during NREM sleep*.** Raw signals were down-sampled to 1.25 kHz and bandpass filtered between 100-600 Hz. Sharp-wave ripple events were detected by thresholding (>3 SDs) the filtered signals using ripple detection scripts from Valero et al (2017). Time-frequency analysis of ripples was calculated using multitaper spectral estimation and frequency resolution of 10 Hz in the 100-600 Hz range.

Statistical Analyses

This study generated a large dataset of neurophysiological measures across several experimental conditions (quiet wake, NREM and REM sleep, memory performance, post-EGCG) in two genotypes. These data and their corresponding statistical results can be found in the SI Appendix. All data is represented as the mean ± SEM. We used paired, unpaired T tests and repeated measures ANOVAs to compare measures across genotypes and to assess the effects of EGCG on trisomic animals. We used Bonferroni correction or Tukey HSD post-hoc tests in the ANOVAs when appropriate. To identify significant correlations between LFP measures and DIs, Pearson or Spearman correlations were used for parametric and non-parametric distributions, respectively. Multiple regression models were used to estimate the relative contribution of LFP measures to memory performance.

REFERENCES

Bokil H, Andrews P, Kulkarni JE, Mehta S, Mitra PP (2010) Chronux: a platform for analyzing neural signals. *J Neurosci Methods* 192(1):146–51.

Gener T, et al. (2019) Serotonin 5-HT1A, 5-HT2A and dopamine D2 receptors strongly influence prefronto-hippocampal neural networks in alert mice: Contribution to the actions of risperidone. *Neuropharmacology* 158:107743.

Gulinello M, et al. (2018) Rigor and reproducibility in rodent behavioral research. *Neurobiol Learn Mem* S1074-7427(18):30001–7.

Hardmeier M, et al. (2014) Reproducibility of functional connectivity and graph measures based on the phase lag index (PLI) and weighted phase lag index (wPLI) derived from high resolution EEG. *PLoS One* 9(10):e108648.

Leger M, et al. (2013) Object recognition test in mice. *Nat Protoc* 8(12):2531–7.

McShane BB, et al. (2012) Assessing REM sleep in mice using video data. *Sleep* 35(3):433–442.

Nolte G, Ziehe A, Nikulin VV, Schlögl A, Krämer N, Brismar T, Müller KR (2008) Robustly estimating the flow direction of information in complex physical systems. *Phys Rev Lett.* 100(23):234101.

Tort ABL, Komorowski R, Eichenbaum H, Kopell N (2010) Measuring phase-amplitude coupling between neuronal oscillations of different frequencies. *J Neurophysiol* 104:1195–1210.

Valero M, Averkin RG, Fernandez-Lamo I, Aguilar J, Lopez-Pigozzi D, Brotons-Mas JR, Cid E, Tamas G, Menendez de la Prida L (2017) Mechanisms for selective single-cell reactivation during offline sharp-wave ripples and their distortion by fast ripples. *Neuron* 94(6):1234-1247.e7

Vinck M, Oostenveld R, Wingerden M Van, Battaglia F, Pennartz CMA (2011) An improved index of phase-synchronization for electrophysiological data in the presence of volume-conduction, noise and sample-size bias. *Neuroimage* 55(4):1548–1565.